Pure valley current and negative differential resistance in optoelectronic superlattices based on monolayer transition metal dichalcogenides

Dan-Na Liu and Yong Guo*

Department of Physics and State Key Laboratory of Low-Dimensional Quantum Physics, Tsinghua University, Beijing 100084, People's Republic of China

(Received 15 March 2022; revised 1 July 2022; accepted 5 July 2022; published 12 July 2022)

We investigate the possibility of achieving valley filtering and enhanced negative differential resistance (NDR) in transition metal dichalcogenide (TMD)-based optoelectronic superlattice (SL). The multipeak NDR is predicted to occur in this system, the operation window of which is controlled successively by the resonant tunneling through miniband regime and the Wannier-Stark ladder regime. It is shown that the synergy of the electric and light stimulus can bring the pure valley current and pronounced peak-to-valley current ratio (PVCR). Our findings illustrate the origin of multipeak responses and provide a theoretical basis for designing devices that can generate pure valley current with complex NDR characteristics.

DOI: 10.1103/PhysRevB.106.035411

I. INTRODUCTION

Negative differential resistance (NDR) refers to the non-Ohmic behavior within a certain range of voltages [1], which can realize fast switching in electronic devices. Devices based on NDR have been widely used in Esaki diodes [2,3], resonant tunneling diodes [4–8], and molecular devices [9–11]. Depending on the physical system, there are many mechanisms for generating NDR, such as resonant electronic tunneling [12–14], interaction between localized narrow energy states [15,16], and suppression from the electrode-molecular region [17]. Given the peculiar ballistic transport properties of relativistic particles in two-dimensional (2D) materials [18,19] and the potential for high-speed electronic applications, it sounds attractive to investigate the possibility of generating and regulating the NDR effect in 2D materials. One stunning 2D material is monolayer transition metal dichalcogenide (TMD), a newly discovered semiconductor that has a wide range of applications in the field of optoelectronics [20]. There are tremendous work on monolayer TMD due to its unique electronic properties, including a relatively large energy gap [21], strong spin-orbit interaction [22], and blocked spin-valley relationship [23]. In the last few years there is a trend of studying NDR effect in TMD systems with both theoretical and experimental progresses [24–29]. Nourbakhsh *et al.* [30] studied the transport properties in both vertical and in-plane directions of MoS_2/WSe_2 heterostructures. The junction shows distinct NDR at room temperature, which results from the band-to-band tunneling at the edge of the MoS_2/WSe_2 heterojunction. Additionally, Liu *et al.* [31] built a WSe_2-based transistor by using metals with different work functions to form electrodes. In contrast to the van der Waals heterojunction comprised of two different 2D materials, the junction shows a strong tunneling current and remarkable NDR behavior. Moreover, an artificial superlattice (SL) formed by periodic external field modulation is an effective way to engineer the transport properties [32]. SL-based diodes with multipeak characteristics have been used in various applications such as in multivalued logic, analog-to-digital convert, and multivalued memory circuits. These devices can perform more logical operations than devices that produce a single NDR peak. In addition, they have the advantage of reducing circuit complexity due to the nature of multiple switching. To form the SL with periodic potential, there are several avenues: gate voltage, magnetic field, off-resonant circularly polarized light (CPL) field, etc. Till now, related schemes based on graphene [33,34], silicene [35–37], MoS_2 [38], and WSe_2 [39], have been proposed. However, the influence of the CPL on the 2D material is an emerging topic, which is promising of realizing valleytronics, and the prediction has been confirmed by experiments with MoS_2 [40] and WSe_2 [41]. Very recently we proposed the CPL- and gate voltage-modulated monolayer WSe_2 double barrier, and found that the valley switching could be efficiently controlled [39]. Surprisingly, so far there is still a lack of investigation of the valley-dependent NDR effect based on the TMD optoelectronic SL.

In this work we report the NDR feature in TMD optoelectronic SL. It is shown that the valley-dependent resonant region and transmission gap are strongly dependent on the bias voltage and the light field. The I-V characteristics exhibit multipeak and valley filtering features under cooperative operations of the back gate electric and the light fields. Moreover, we find that the peak-to-valley current ratio (PVCR) can be enhanced in the SL.

II. MODEL AND METHODS

The TMD optoelectronic SL is shown in Fig. 1, which can be realized by periodically applying the back gate electric field and the off-resonant CPL to the modulated regions. The metal

*guoy66@tsinghua.edu.cn

electrodes on both sides of the TMD sheet create a linear electrostatic potential drop along x direction. We choose WSe_2 as the prototypical representative which is a semiconductor with a direct band gap of about 850 meV, and the following results can be extended to other TMD materials. The effective Hamiltonian of monolayer WSe_2 in normal and modulated regions ($j = W, B$) can be written as [32]

$$H_j = \upsilon_f(\eta\sigma_x p_x + \sigma_y p_y) + (\Delta + \eta\Omega_j)\sigma_z + \eta s_z(\lambda_c\sigma_+ + \lambda_v\sigma_-) + U(x), \quad (1)$$

where $\upsilon_F \approx 5 \times 10^5$ m/s is the Fermi velocity, $\eta = \pm 1$ is the valley index, $s_z = \pm 1$ is the spin index, $\sigma_i (i = x, y, z)$ is the Pauli matrix, $\Delta = 850$ meV represents the band gap, $\lambda_{c(v)} = 7.5(112.5)$ meV is the SOC for the conduction (valence) band, and $\sigma_\pm = \sigma_0 \pm \sigma_z$ (σ_0 is the identity matrix). $U(x)$ is the position dependent electrostatic potential energy that has two parts: first, the Kronig-Penney-type potential that takes as zero in normal regions and U in modulated regions. The second is $f = eV_B/L$ that is contributed by bias (V_B is the electric field and L is the channel length):

$$U(x) = \begin{cases} U - fx, & \text{modulated regions,} \\ -fx, & \text{normal regions,} \end{cases} \quad (2)$$

The dynamics of an electron under optoelectronic action can be reduced to that of an electron under effective potential $U_{\text{eff}}^{\eta,s_z}(x)$. Here

$$U_{\text{eff}}^{\eta,s_z}(x) = \begin{pmatrix} \Delta + \eta\Omega_j + 2\eta s_z\lambda_c + U(x) & 0 \\ 0 & -(\Delta + \eta\Omega_j) + 2\eta s_z\lambda_v + U(x) \end{pmatrix}. \quad (3)$$

From Eq. (3) we can obtain that the $U_{\text{eff}}^{\eta,s_z}(x)$ for $s_z = 1(-1)$ is $U_{\text{eff}}^{\eta,\uparrow(\downarrow)} = \pm(\Delta + \eta\Omega_j) + 2\eta\lambda_{c(v)} + U(x)$. In Fig. 1(b) we show the valley-dependent effective potential for $s_z = 1$ under bias with considering vertical electric and light stimuli, which help us better understand the mechanism of the valley filter.

According to the Floquet theory [42], when both off-resonant condition $\hbar\omega \gg t$ and the limit of $eA\upsilon_F/\hbar\omega \ll 1$ are satisfied, the influence of such light field to the Hamiltonian near Dirac point can be reduced to the static effective term $\Omega = (eA\upsilon_F)^2/\hbar\omega$, with $\Omega > 0$ (<0) corresponding to the right (left) circular polarization, where ω is the frequency of light, and A is the scalar potential of external electromagnetic potential from CPL. We set $\Omega_W = 0$, $\Omega_B \neq 0$. Explicitly H_j is given by

$$H_j = \begin{pmatrix} \delta_j^c + U(x) - E & \hbar\upsilon_F(-i\eta\partial_x - \partial_y) \\ \hbar\upsilon_F(-i\eta\partial_x + \partial_y) & \delta_j^v + U(x) - E \end{pmatrix}, \quad (4)$$

where $\delta_j^c = \Delta + \eta\Omega_j + 2\eta s_z\lambda_c$ and $\delta_j^v = -\Delta - \eta\Omega_j + 2\eta s_z\lambda_v$.

The differential equation $H_j\Psi_j = E\Psi_j$ admits the solution of eigenstates $\Psi_j(x)e^{ik_y y}$ with

$$\Psi_j(x) = \begin{pmatrix} e^{ik_j x} & e^{-ik_j x} \\ G_j e^{ik_j x} & -G_j^* e^{-ik_j x} \end{pmatrix}\begin{pmatrix} \mu_j \\ \rho_j \end{pmatrix}, \quad (5)$$

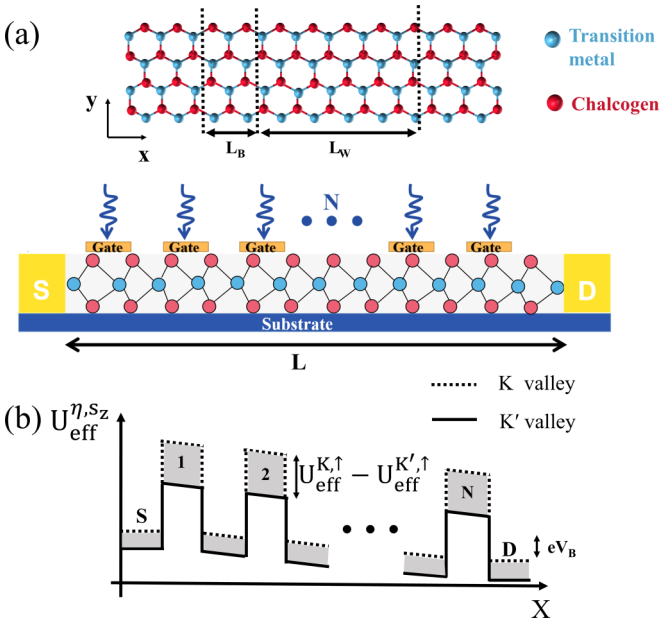

FIG. 1. (a) Schematic illustration of the TMD optoelectronic superlattice with period number N, barrier (well) width L_B (L_W), and channel length L. (b) The valley-dependent effective potential energy for $s_z = 1$ under bias with considering vertical electric and light stimuli.

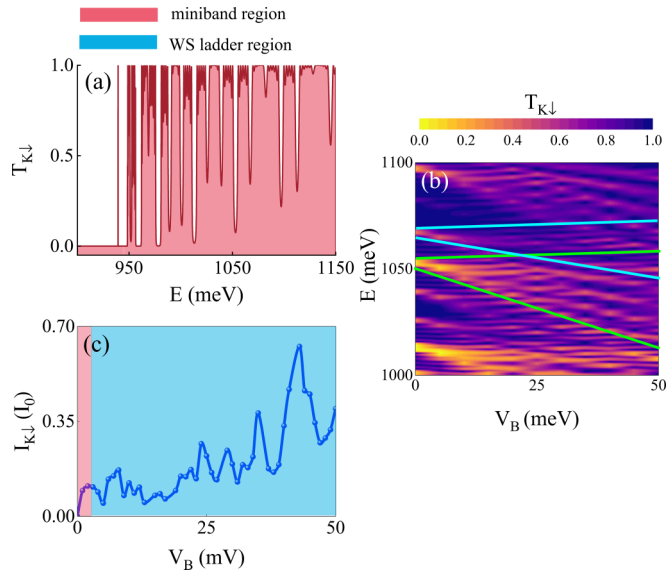

FIG. 2. (a) $T_{K\downarrow}$ without bias. When electrons move in Kronig-Penney potential, the resonance level widens to miniband with the transmission of nearly 1. (b) Map of $T_{K\downarrow}$ spectrum, showing the destruction of the minibands into WS ladders and the hybridization of WS ladders in different minibands with increasing bias. (c) $I_{K\downarrow}$-V_B characteristic. Minibands, WS ladders, and hybridization between WS ladders are responsible for multipeak NDR. $N = 6$, $L_B = 10$ nm, $L_W = 30$ nm, $\Omega = 10$ meV, and $U = 100$ meV.

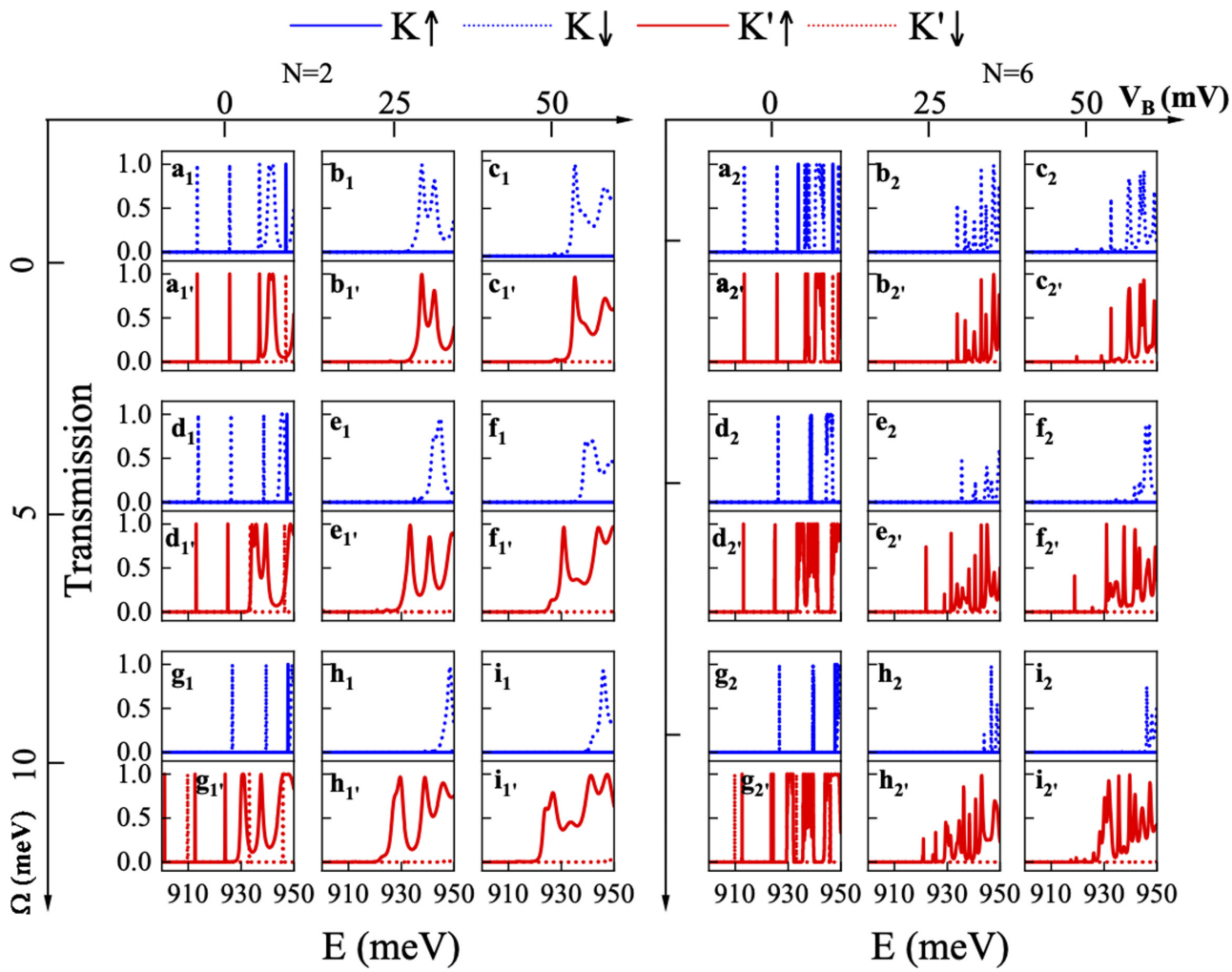

FIG. 3. Transmission as a function of the incident energy under different values of the bias voltage and the light-induced gap of the CPL for (a_1)–$(i_{1'})$: $N = 2$, and (a_2)–$(i_{2'})$: $N = 6$. $L_B = 10$ nm, $L_W = 30$ nm, $U = 100$ meV, and $\theta = 0$.

where

$$G_j = \frac{\hbar v_F(-\eta k_j - ik_y)}{\delta_j^v + U(x) - E},$$
$$k_y = \sqrt{(\delta_W^c - E)(\delta_W^v - E)/(\hbar v_F)^2}\sin\theta,$$
$$k_j = \sqrt{[\delta_j^c + U(x) - E][\delta_j^v + U(x) - E]/(\hbar v_F)^2 - k_y^2}. \tag{6}$$

The wave function in periodic SL system without bias is a Bloch function and the dispersion relation can be derived by the pertinent transfer-matrix method (TMM). The transfer matrix (TM) is expressed as

$$M = \frac{(\delta_W^v - E)(\delta_B^v + U - E)}{4(\hbar v_F)^2 k_W k_B}\begin{pmatrix}\Lambda & \lambda\\ \lambda^* & \Lambda^*\end{pmatrix} \tag{7}$$

with

$$\Lambda = (G^* + H)(H^* + G)e^{ik_W L_W}e^{ik_B L_B} + (-G^* + H^*)(-H + G)e^{ik_W L_W}e^{-ik_B L_B},$$
$$\lambda = -2i(G^* + H)(G - H^*)e^{ik_W(L_B + L_W)}\sin(k_B L_B), \tag{8}$$

then the dispersion relation can be constructed as

$$\cos(Kl) = \frac{(\delta_W^v - E)(\delta_B^v + U - E)}{4(\hbar v_F)^2 k_W k_B} \times (G^* + H)(H^* + G)\cos(-k_W L_W - k_B L_B) + (-G^* + H^*)(-H + G)\cos(-k_W L_W + k_B L_B). \tag{9}$$

The external potential is the variable that depends on position x under bias. To apply TMM for this SL structure, we can divide the whole junction into n small regions, where the potential energy of each region is regarded as a constant U_n, and the TM in xth region is

$$M_n(x_n) = \begin{pmatrix} e^{ik_n x_n} & e^{-ik_n x_n}\\ G_n e^{ik_n x_n} & -G_n^* e^{-ik_n x_n}\end{pmatrix}^{-1} \times \begin{pmatrix} e^{ik_{n+1}x_n} & e^{-ik_{n+1}x_n}\\ G_{n+1}e^{ik_{n+1}x_n} & -G_{n+1}^* e^{-ik_{n+1}x_n}\end{pmatrix}. \tag{10}$$

TM of the whole system connecting source and drain is

$$T_M = \prod_n M_n(x_n), \tag{11}$$

and we obtain the transmission coefficient t_{η,s_z}, then the transmission probability reads

$$T_{\eta,s_z} = \frac{k_R}{k_L}\frac{\delta_w^v - E}{\delta_w^v - E - eV_B}\left|t_{\eta,s_z}\right|^2 \tag{12}$$

with

$$k_L = \sqrt{\left(\delta_w^c - E\right)\left(\delta_w^v - E\right)/(\hbar\upsilon_F)^2 - k_y^2},$$
$$k_R = \sqrt{\left(\delta_w^c - eV_B - E\right)\left(\delta_w^v - eV_B - E\right)/(\hbar\upsilon_F)^2 - k_y^2}. \tag{13}$$

The spin- and valley-dependent current at zero temperature is given by [43]

$$I_{\eta,s_z} = I_0\int_{E_F - eV_B}^{E_F}\int_{-\pi/2}^{\pi/2} T_{\eta,s_z}|E|dE\cos\theta d\theta, \tag{14}$$

where θ is the incident angle, E_F is the Fermi energy, and here we set $E_F = 950$ meV. The valley current can be defined as $I_{K(K')} = I_{K(K')\uparrow} + I_{K(K')\downarrow}$, the total current is $I_t = I_K + I_{K'}$, and the valley polarization of current is $P_V = (I_K - I_{K'})/I_t$.

III. RESULTS AND DISCUSSIONS

In Fig. 2 we first illustrate the mechanism of generating multipeak NDR in SL structure. When the electron moves in the periodic potential without bias, due to the influence of the two adjacent quantum wells, the wave function of each energy level in the two wells is combined in a symmetric or antisymmetric way, and then each energy level is correspondingly split into two. Thus, when many square wells come close to each other to form the Kronig-Penney (KP) potential, each energy level of the original spectrum of electrons moving in this potential will split and widen into the miniband [see Fig. 2(a)], which is the most important feature of electron motion in the crystal.

In the presence of a uniform electric field, the dynamics of the electrons in the KP potential is described by Bloch oscillations. The interference between electron wave packets destroys the miniband into the localized Wannier-Stark (WS) ladder [see Fig. 2(b)], which suppresses the tunneling of electrons, causing the decreasing of current and the first current peak [see Fig. 2(c)]. With the sweep of bias voltage, the interaction of branching from different WS ladders is responsible for multipeak NDR.

The effects of the CPL and the bias voltage on the valley-dependent transport properties of simple ($N = 2$) and complex ($N = 6$) structures are investigated and shown in Fig. 3. For $\Omega = 0$, the degeneracy of K and K' valleys is not lifted [see Figs. 3(a_1), and 3($a_{1'}$)]. As Ω increases, the splitting of valley degree of freedom becomes significant and the transmission shows the effect of valley-dependent resonant enhancement or suppression. In contrast to the transmission spectra at $\Omega = 5$ meV [see Figs. 3(d_1) and 3($d_{1'}$)], the transmission spectra at $\Omega = 10$ meV shows significant resonant enhancement for the K' valley, but resonant suppression for the K valley [see Figs. 3(g_1) and 3($g_{1'}$)]. That is, the number of resonant peaks for K' valley increases, the resonant region becomes wider, and the nonresonant region becomes

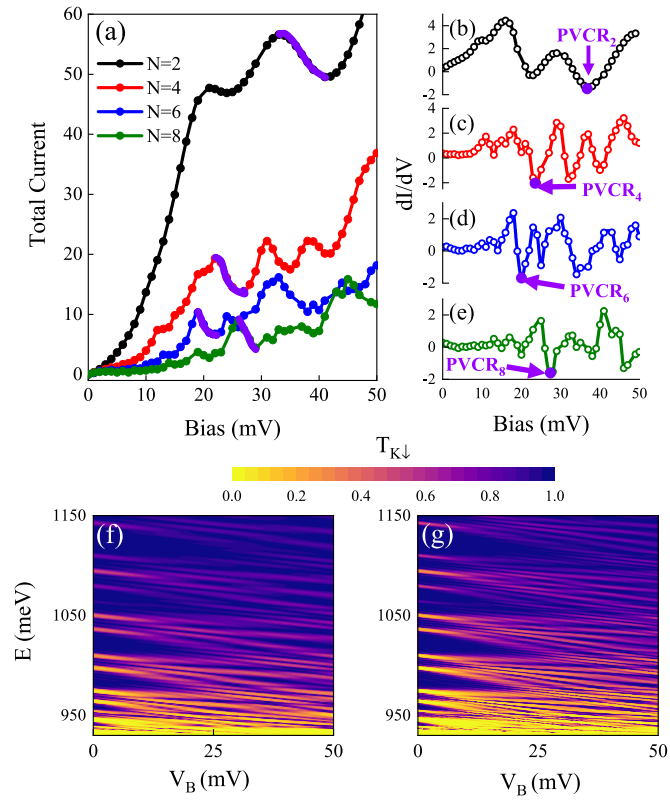

FIG. 4. (a) Total current-voltage and (b)–(e) dI/dV characteristics with variation of N. In (a), the regions that produce maximum PVCR_N are highlighted in purple, which corresponds to the minimum points of the dI/dV curves in the negative range of the ordinate (marked with purple arrows) in (b)–(e). (f) and (g) $T_{K\downarrow}$ for $N = 4$ and $N = 6$, respectively. $L_B = 10$ nm, $L_W = 30$ nm, $\Omega = 0$ meV, and $U = 100$ meV.

narrower, while the resonant peaks for K valley decrease and the transmission gap gets wider. The Hamiltonian revealed in Eq. (1) can show the physical mechanism of the above transport phenomena. In the case of $\Omega = 0$, $\eta\Omega = 0$ leads to the particles tunneling with the degenerate valley index between the source and drain, resulting in the preservation of valley degeneracy in the transmission spectra. When $\Omega > 0$, the valley degeneracy is lifted, and the resonant band and transmission gap in the transmission spectra are coherent with the valley index. Moreover, we find that the right circular polarization strengthen (weaken) the band gap of K (K') valley, which is responsible for the resonant suppression (enhancement) effect of transport.

In Fig. 3, along the V_B axis, we exhibit the evolution of the valley-dependent transport behavior under bias regulation. At $V_B = 0$, the transmission spectra coincide with the picture of perfect resonant tunneling, in which the resonant tunneling predicts the positions of quasieigenstate energy in the interacting quantum well structure. Furthermore, the transmission spectra at zero bias show that for a specific valley, the intervals of resonant and nonresonant bands for spin-up particles are greatly misaligned with those for spin-down ones. This phenomenon is consistent with the spin filtering nature in the electric superlattice we predicted in Ref. [32]. When V_B increases, it can be observed that (1) transmission spectra

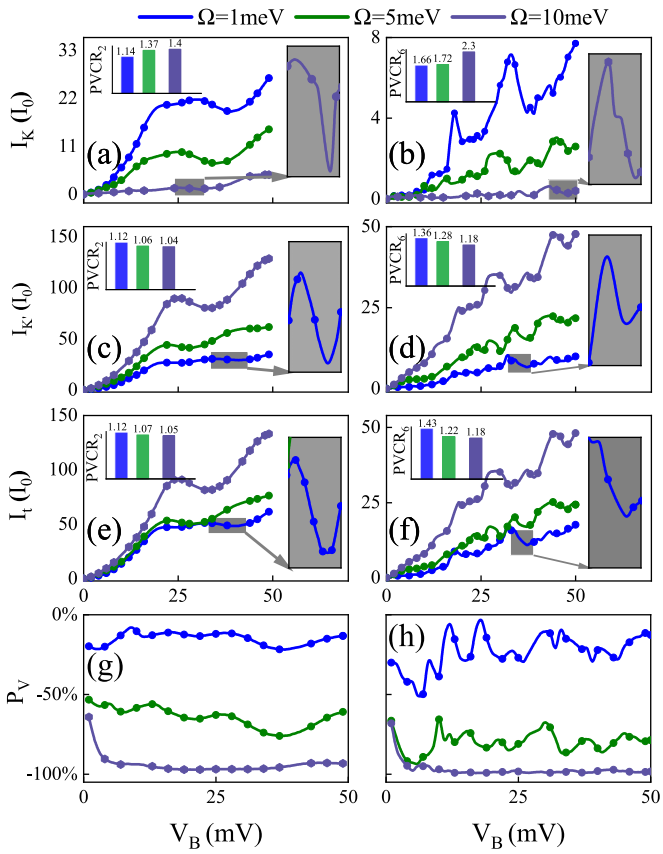

FIG. 5. I-V_B characteristics for various Ω. (a) and (b) K valley current; (c) and (d) K' valley current; (e) and (f) total current; (g) and (h) valley polarization of current. The insets depict the PVCR$_N$ vs Ω. $N = 2$ for the left panel, and $N = 6$ for the right panel. $L_B = 10$ nm, $L_W = 30$ nm, and $U = 100$ meV.

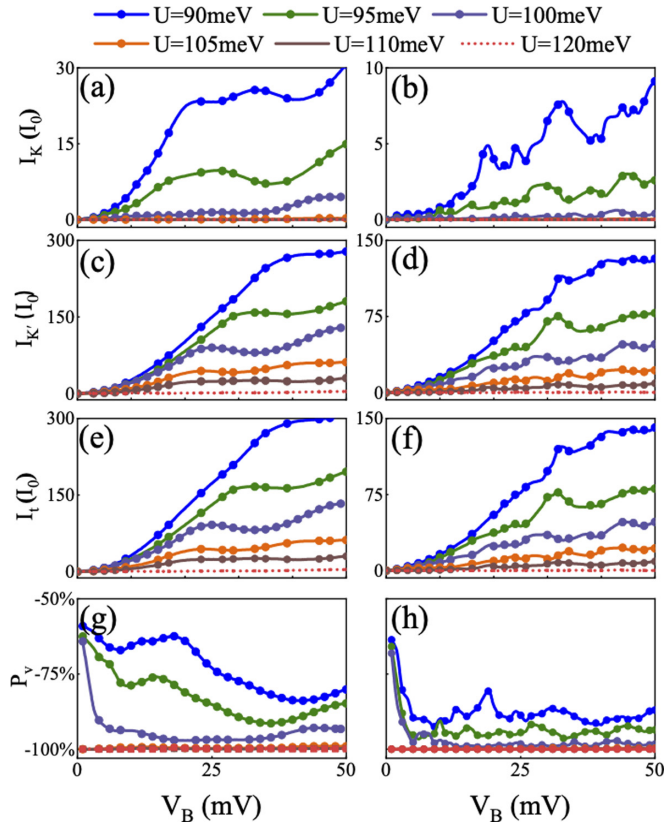

FIG. 6. I-V_B characteristics for various U. (a) and (b) K valley current; (c) and (d) K' valley current; (e) and (f) total current; (g) and (h) valley polarization of current. $N = 2$ for the left panel and $N = 6$ for the right panel. $L_B = 10$ nm, $L_W = 30$ nm, and Ω = 10 meV.

present suppressed evolution, (2) broadening of transmission gap for both K and K' valley in the lower energy regime [see Figs. 3(b$_2$) and 3(b$_{2'}$)], and meanwhile (3) the transmission peak values are reduced in the higher energy regime [see Figs. 3(c$_2$) and 3(c$_{2'}$)]. The mechanism underlying these phenomena is that the bias causes the destruction of miniband to WS ladder, leading to the inhibition of tunneling.

Figure 4 presents the I_t-V_B characteristics in the case of zero optical field for structures with different period number $N = 2$, 4, 6, and 8. It should be noted that, within the range of low bias ($V_B < 20$ mV), the total current changes almost linearly with V_B. It is evident that further increasing bias leads to reduction in current and apparent NDR effect. Interestingly, the study shows a continuous reduction of the current with increasing N. To analyze the sensitivity of the current to N, we further plot the transmission related to energy and bias for $N = 4$ and $N = 6$, as shown in Figs. 4(f) and 4(g). As can be seen, the suppression region is significantly enlarged when N increases, which leads to the lowered transmission contribution to the current window, thus reducing the current.

The significance of NDR effect for period number N can be qualitatively described by the PVCR$_N$, here we only compare the maximum PVCR in I_t-V_B. In order to analyze whether there exists NDR, we further plot the dI/dV diagrams in Figs. 4(b)–4(e). As can be seen, dI/dV shows oscillatory behavior with the change of bias. Note that the dI/dV realizes the minimum value in the negative range (marked with purple arrows), indicating that a maximum PVCR occurs around this bias. From $N = 2$ to $N = 8$, the corresponding maximum PVCRs are 1.142, 1.393, 1.52, and 2.02, respectively. As N increases, the rising PVCR indicates that the SL can enhance the NDR effect. In the complicated SL discussed, and the bias voltage is not considered, the coupling of resonant energy levels between layers is the reason for the nearly linear current. Upon modulation by the bias, the matching of resonant modes is reduced, resonant tunneling is suppressed, the minibands are broken into WS ladders, which leads to the reduction of current. When the bias voltage increases further, the WS ladders in different minibands produce a new set of current peaks by hybridization.

Figure 5 shows the valley-dependent current, total current, and corresponding valley polarization as a function of the bias voltage for different values of Ω. The left and right panels are for $N = 2$ and $N = 6$, respectively. Several obvious phenomena appear: First, when $N = 6$, for both $I_{K(K')}$ and I_t, weaker current, more peaks, and relatively strong PVCR (see the insets in Fig. 5) are observed compared with those for $N = 2$, which further validates the feasibility and practicability of utilizing SL system to achieve multipeak effect and improve NDR performance. Second, the valley polarization of current in complex structure shows multipeak effect [see Fig. 5(h)]. Third, strong light field suppresses the K valley current, but

enhances the K' valley current, the total current, and the valley polarization. As shown in Figs. 5(g) and 5(h), P_V approaches -100% and thus the pure valley current is achieved for the case of $\Omega = 10$ meV. Our method opens up the possibility of optical manipulation on valley index and generating pure valley current in the SL system. Similar to spin current, such a pure valley current contributes to eliminating charge-related effect [44,45] and producing minimal Joule heating [46].

In Fig. 6 we show the $I_{K(K')}$-, I_t-, and P_V-V_B characteristics of WSe_2 SL for different values of gate voltage U. The left (right) panel corresponds to $N = 2$ ($N = 6$). Figures 6(a)–6(f) show that by changing the gate voltage, both the valley current and the total current display a similar trend. Increasing U from 90 to 100 meV, the current drops dramatically, which is physically understandable due to the enlarged band gap induced by the gate voltage that hinders the passage of particles. When the gate voltage continue increasing, the current is eventually suppressed to zero over a relatively wide range of bias, due to that it is difficult to cross particles when the Fermi lever fails into the band gap. Moreover, the NDR effect is affected by the gate voltage. In our calculation, the NDR effect is the most salient for $U = 90$ and 95 meV when $N = 6$. Additionally, changing the gate voltage also affects the polarization of the current. As seen in Figs. 6(g) and 6(h), whether for simple structure ($N = 2$) or SL ($N = 6$), increasing the gate voltage will enhance the effect of the valley current filtering.

IV. CONCLUSIONS

In summary, we theoretically studied the multipeak NDR feature in TMD-based optoelectronic SL and demonstrated that the SL structure can enhance the PVCR. These characteristics are dominated by the miniband regime in lower bias and Wannier-Stark regime in higher bias. We also found that the appropriate parameters of back gate electric and optical fields are necessary for generating the pure valley current. This work provides an effective strategy for manipulating the valley-dependent NDR effect in the SL structure based on monolayer TMD.

ACKNOWLEDGMENT

This work was supported by the National Natural Science Foundation of China under Grant No. 12074209.

[1] L. L. Chang, L. Esaki, and R. Tsu, Appl. Phys. Lett. **24**, 593 (1974).
[2] R. Yan, S. Fathipour, Y. Han, B. Song, S. Xiao, M. Li, N. Ma, V. Protasenko, D. A. Muller, D. Jena, and H. G. Xing, Nano Lett. **15**, 5791 (2015).
[3] A. V. Bruce, S. L. Liu, J. N. Fry, and H. P. Cheng, Phys. Rev. B **102**, 115415 (2020).
[4] C. Bayram, Z. Vashaei, and M. Razeghi, Appl. Phys. Lett. **97**, 092104 (2010).
[5] T. A. Growden, D. F. Storm, W. D. Zhang, E. R. Brown, D. J. Meyer, P. Fakhimi, and P. R. Berger, Appl. Phys. Lett. **109**, 083504 (2016).
[6] K. Xu, E. Wynne, and W. J. Zhu, Adv. Electron. Mater. **6**, 2000318 (2020).
[7] G. C. Constantinescu and N. D. M. Hine, Nano Lett. **16**, 2586 (2016).
[8] P. M. Campbell, A. Tarasov, C. A. Joiner, W. J. Ready, and E. M. Vogel, ACS Nano **9**, 5000 (2015).
[9] E. D. Mentovich, I. Kalifa, A. Tsukernik, A. Caster, N. Rosenberg-Shraga, H. Marom, M. Gozin, and S. Richter, Small **4**, 55 (2008).
[10] J. Chen, M. A. Reed, A. M. Rawlett, and J. M. Tour, Science **286**, 1550 (1999).
[11] M. Q. Long, K. Q. Chen, L. L. Wang, W. Qing, B. S. Zou, and Z. Shuai, Appl. Phys. Lett. **92**, 243303 (2008).
[12] Z. K. Tang and X. R. Wang, Appl. Phys. Lett. **68**, 3449 (1996).
[13] D. Dragoman and M. Dragoman, Appl. Phys. Lett. **90**, 143111 (2007).
[14] B. Hsu, S. Farid, J. Almazan, M. A. Stroscio, and M. Dutta, Appl. Phys. Lett. **118**, 063102 (2021).
[15] L. Chen, Z. P. Hu, A. D. Zhao, B. Wang, Y. Luo, J. L. Yang, and J. G. Hou, Phys. Rev. Lett. **99**, 146803 (2007).
[16] I. W. Lyo and P. Avouris, Science **245**, 1369 (1989).
[17] Y. D. Guo, J. J. Wang, H. L. Zeng, Y. S. Ran, Z. C. Liang, and X. H. Yan, J. Appl. Phys. **128**, 184301 (2020).
[18] G. Auton, J. W. Zhang, R. K. Kumar, H. B. Wang, X. J. Zhang, Q. P. Wang, E. Hill, and A. M. Song, Nat. Commun. **7**, 11670 (2016).
[19] I. S. Bhatia and D. K. K. Randhawa, Curr. Sci. **118**, 1656 (2020).
[20] A. Ciarrocchi, A. Avsar, D. Ovchinnikov, and A. Kis, Nat. Commun. **9**, 919 (2018).
[21] K. F. Mak, C. G. Lee, J. Hone, J. Shan, and T. F. Heinz, Phys. Rev. Lett. **105**, 136805 (2010).
[22] D. Xiao, G. B. Liu, W. X. Feng, X. D. Xu, and W. Yao, Phys. Rev. Lett. **108**, 196802 (2012).
[23] Y. Ye, J. Xiao, H. L. Wang, Z. L. Ye, H. Y. Zhu, M. Zhao, Y. Wang, J. H. Zhao, X. B. Yin, and X. Zhang, Nat. Nanotechnol. **11**, 598 (2016).
[24] P. M. Campbell, A. Tarasov, C. A. Joiner, W. J. Ready, and E. M. Vogel, J. Appl. Phys. **119**, 024503 (2016).
[25] A. Sengupta and S. Mahapatra, J. Appl. Phys. **114**, 194513 (2013).
[26] K. Takeyama, R. Moriya, S. Okazaki, Y. Zhang, S. Masubuchi, K. Watanabe, T. Taniguchi, T. Sasagawa, and T. Machida, Nano Lett. **21**, 3929 (2021).
[27] W. Choi, S. Hong, Y. Jeong, Y. Cho, H. G. Shin, J. H. Park, Y. Yi, and S. Im, Adv. Funct. Mater. **31**, 2009436 (2021).
[28] N. Papadopoulos, P. Gehring, K. Watanabe, T. Taniguchi, H. S. J. van der Zant, and G. A. Steele, Phys. Rev. B **101**, 165303 (2020).
[29] M. Wang, C. Y. Wang, C. C. Wu, Q. Li, C. Pan, C. Wang, S. J. Liang, and F. Miao, Adv. Electron. Mater. **5**, 1800853 (2019).
[30] A. Nourbakhsh, A. Zubair, M. S. Dresselhaus, and T. Palacios, Nano Lett. **16**, 1359 (2016).
[31] C. S. Liu, X. Yan, E. Z. Zhang, X. F. Song, Q. Q. Sun, S. J. Ding, W. Z. Bao, F. X. Xiu, P. Zhou, and D. W. Zhang, Small **13**, 1604319 (2017).
[32] D. N. Liu and Y. Guo, Appl. Phys. Lett. **118**, 123101 (2021).

[33] G. J. Ferreira, M. N. Leuenberger, D. Loss, and J. C. Egues, Phys. Rev. B **84**, 125453 (2011).
[34] J. Munárriz, C. Gaul, A. V. Malyshev, P. A. Orellana, C. A. Müller, and F. Domínguez-Adame, Phys. Rev. B **88**, 155423 (2013).
[35] C. H. Chen, W. W. Li, Y. M. Chang, C. Y. Lin, S. H. Yang, Y. Xu, and Y. F. Lin, Phys. Rev. Appl. **10**, 044047 (2018).
[36] S. M. Sattari-Esfahlan, J. Appl. Phys. **123**, 244503 (2018).
[37] X. S. Wang, M. Shen, X. T. An, and J. J. Liu, Phys. Lett. A **380**, 1663 (2016).
[38] X. J. Qiu, Z. Z. Cao, Y. F. Cheng, and C. C. Qin, J. Phys.: Condens. Matter **29**, 105301 (2017).
[39] D. N. Liu, B. Y. Liu, R. Y. Yuan, J. Zheng, and Y. Guo, Phys. Rev. B **103**, 245432 (2021).
[40] H. L. Zeng, J. F. Dai, W. Yao, D. Xiao, and X. D. Cui, Nat. Nanotechnol. **7**, 490 (2012).
[41] W. T. Hsu, Y. L. Chen, C. H. Chen, P. S. Liu, T. H. Hou, L. J. Li, and W. H. Chang, Nat. Commun. **6**, 1 (2015).
[42] T. Kitagawa, T. Oka, A. Brataas, L. Fu, and E. Demler, Phys. Rev. B **84**, 235108 (2011).
[43] M. Büttiker, Y. Imry, R. Landauer, and S. Pinhas, Phys. Rev. B **31**, 6207 (1985).
[44] F. J. Jedema, A. T. Filip, and B. J. Van Wees, Nature (London) **410**, 345 (2001).
[45] T. Yang, T. Kimura, and Y. Otani, Nat. Phys. **4**, 851 (2008).
[46] W. Y. Shan, J. H. Zhou, and D. Xiao, Phys. Rev. B **91**, 035402 (2015).